

High performance Ga As Sb / Ga As quantum well lasers

S.-Q. Yu, D. Ding, J.-B. Wang, N. Samal, X. Jin, Y. Cao, S. R. Johnson, and Y.-H. Zhang

Citation: *Journal of Vacuum Science & Technology B* **25**, 1658 (2007); doi: 10.1116/1.2781531

View online: <http://dx.doi.org/10.1116/1.2781531>

View Table of Contents: <http://scitation.aip.org/content/avs/journal/jvstb/25/5?ver=pdfcov>

Published by the AVS: Science & Technology of Materials, Interfaces, and Processing

Articles you may be interested in

[Highly tensile-strained, type-II, Ga_{1-x}In_xAs / GaSb quantum wells](#)

Appl. Phys. Lett. **96**, 062109 (2010); 10.1063/1.3303821

[Nitrogen incorporation and optical studies of GaAsSbN/GaAs single quantum well heterostructures](#)

J. Appl. Phys. **102**, 053106 (2007); 10.1063/1.2777448

[Effect of multilayer barriers on the optical properties of GaInNAs single quantum-well structures grown by metalorganic vapor phase epitaxy](#)

Appl. Phys. Lett. **87**, 021903 (2005); 10.1063/1.1993758

[Effect of temperature on the optical properties of GaAsSbN/GaAs single quantum wells grown by molecular-beam epitaxy](#)

J. Appl. Phys. **93**, 4475 (2003); 10.1063/1.1560574

[Growth of high-quality GaAs/AlAs Bragg mirrors on patterned InP-based quantum well mesa structures](#)

Appl. Phys. Lett. **71**, 581 (1997); 10.1063/1.119800



SHIMADZU Excellence in Science

Powerful, Multi-functional UV-Vis-NIR and FTIR Spectrophotometers

Providing the utmost in sensitivity, accuracy and resolution for applications in materials characterization and nano research

- Photovoltaics
- Polymers
- Thin films
- Paints
- Ceramics
- DNA film structures
- Coatings
- Packaging materials

[Click here to learn more](#)



High performance GaAsSb/GaAs quantum well lasers

S.-Q. Yu,^{a)} D. Ding, J.-B. Wang, N. Samal, X. Jin, Y. Cao, S. R. Johnson, and Y.-H. Zhang
Center for Solid State Electronics Research, Department of Electrical Engineering, Arizona State University, Tempe, Arizona 85287-6206

(Received 19 April 2007; accepted 13 August 2007; published 13 September 2007)

GaAsSb/GaAs quantum wells (QWs) with 1.3 μm light emission are grown using solid-source molecular beam epitaxy. The growth temperature is optimized based on photoluminescence (PL) linewidth and intensity and edge-emitting laser (EEL) threshold current density; these measurements concur that the optimal growth temperature is $\sim 490^\circ\text{C}$ ($\sim 500^\circ\text{C}$) for GaAsSb/GaAs QWs grown with (without) GaAsP strain compensation. High performance EELs and vertical-cavity surface-emitting lasers (VCSELs) are demonstrated using the GaAsSb/GaAs/GaAsP strain compensated active region. One EEL achieved an output power up to 0.9 W with thresholds as low as 356 A/cm² under room temperature pulsed operation, while another achieved continuous-wave (cw) operation at temperatures up to 48 $^\circ\text{C}$ for wavelengths as long as 1260 nm. A set of VCSELs achieved room temperature cw operation with output powers from 0.03 to 0.2 mW and lasing wavelengths from 1240 to 1290 nm. The temperature characteristics of these devices indicate that the optimal gain-peak cavity-mode tuning for pulsed operation specifies a room temperature PL peak redshift of 20–30 nm relative to the cavity mode.
© 2007 American Vacuum Society. [DOI: 10.1116/1.2781531]

I. INTRODUCTION

Vertical-cavity surface-emitting lasers (VCSELs) operating at 1.3 μm are of great interest for low-cost data transmission applications such as fiber to the home, local area networks, and free-space optical interconnects. As the preferred substrate for 1.3 μm VCSELs, GaAs permits the growth of near lattice-matched GaAs/AlGaAs distributed Bragg reflectors (DBRs), which have superior optical and thermal properties when compared to other III-V DBRs. Furthermore, the fabrication of GaAs based 1.3 μm VCSELs can take full advantage of the industrial standard 850 nm VCSEL fabrication technology, which is attractive from a manufacturing point of view. GaAsSb quantum wells (QWs) have been shown to be one of the most suitable candidates for 1.3 μm active regions on the GaAs substrate.^{1–12}

The growth of high quality GaAsSb QWs using molecular beam epitaxy (MBE) can be challenging.^{13–15} GaAsSb QWs are highly strained ($\sim 2.7\%$) at the composition necessary to achieve 1.3 μm emission. The strain not only limits the maximum QW number that can be grown without misfit dislocations but also results in the strain-driven in-plane composition fluctuations that cause inhomogeneous linewidth broadening¹⁴ and reduce internal quantum efficiency. Moreover, the growth of mixed group-V materials requires additional calibration work since the group-V species (As and Sb) have a less than unity sticking coefficient that varies with both growth temperature and the relative flux of each group-V element. The quality of GaAsSb/GaAs QWs for 1.3 μm light emission can be improved by introducing GaAsP strain compensation layers and further optimizing the growth conditions of the resulting five-layer QW system.¹⁴

As a result, high internal quantum efficiency edge-emitting lasers (EELs) and high power VCSELs have been demonstrated using this active region structure.^{8,11,12,16}

Realizing GaAsSb/GaAs based VCSELs can be challenging because a nearly flat conduction band alignment between GaAs and GaAsSb results in the weak confinement of electrons and the strong confinement of holes and a less than ideal electron-hole wave function overlap that limits gain.^{15,17} Furthermore, the combination of limited gain and in-plane composition fluctuations bring about a significant blueshift in the gain peak under injection.¹⁶ This is an important design concern, as the key to good VCSEL performance is the excellent alignment of the gain peak and the cavity mode at the operating temperature. In designing a VCSEL, it is convenient to establish this alignment based on a wavelength difference between the room temperature active region photoluminescence (PL) peak and the cavity mode. For GaAs and InGaAs active materials, the gain-peak position is governed by thermal effects and is insensitive to band filling under high injection. Therefore, the design rule for GaAs or InGaAs VCSELs is to have the room temperature PL peak slightly blueshifted relative to the cavity mode.^{18–20} In which case, the active region heats up under continuous-wave (cw) operation, and since the gain-peak redshift with temperature exceeds that of the cavity mode, the gain peak and cavity mode are aligned at the operating temperature. However, the design rule for GaAsSb VCSELs is not as straightforward since in addition to the thermal induced redshift, there is a substantial gain-peak blueshift due to band filling under high injection.

This article studies the issues related to the optimization and growth of 1.3 μm , strain compensated GaAsSb/GaAs/GaAsP QW structures for laser applications, including the performance characteristics of high power, cw, room

^{a)}Author to whom correspondence should be addressed; electronic mail: yushq@asu.edu

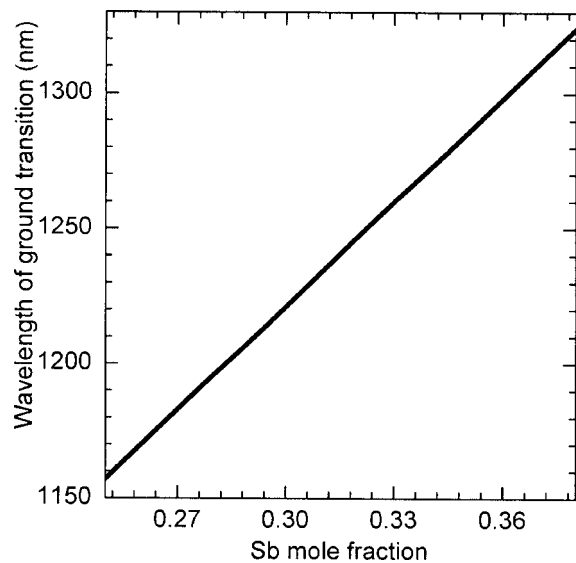


FIG. 1. Calculated wavelength of the first energy transition in a GaAsP/GaAs/GaAsSb/GaAs/GaAsP (9/5/7/5/9 nm) five-layer QW structure as a function of Sb composition.

temperature EELs and VCSELs, and the competing effects of a thermally induced redshift and an injection induced blueshift on the design rules of GaAsSb based VCSELs.

II. STRAIN COMPENSATED GaAsSb QWs

The critical layer thickness for pseudomorphically strained GaAs_{0.6}Sb_{0.4} on GaAs is approximately 7 nm;²¹ critical layer thickness not only limits the thickness of each QW, it also limits the total number of QWs that can be consecutively grown. The latter can be overcome by adding tensile strain layers between the QWs, for which GaAsP is readily available and as well offers enhanced electron confinement when placed either side and near to the GaAsSb/GaAs QW. In this work, a five-layer GaAsP/GaAs/GaAsSb/GaAs/GaAsP strain compensated QW system is developed. The ground-state transition wavelength for this five-layer system with layer thicknesses 9/5/7/5/9 nm is calculated using the transfer-matrix method and plotted as a function of Sb mole fraction in Fig. 1. The material parameters used for GaAs_{1-x}Sb_x are linearly interpolated between those of GaAs and GaSb except the formula for the band gap of unstrained bulk GaAs_{1-x}Sb_x, which has a substantial bowing parameter and is given by¹⁷

$$E_g(x) = 1.43(1 - x) + 0.73 - 1.58x(1 - x). \quad (1)$$

The Sb mole fraction is ~ 0.36 for the light emission at 1.3 μm .

The materials studied in this work are grown by solid-source molecular beam epitaxy using a VG V80H system equipped with As, Sb, and P valved crackers to control the mixed group-V composition of the active layers. To calibrate the composition of GaAsSb layers, two sets of GaAsSb PL samples are studied. These samples contain the above mentioned five-layer QW system, with a 50 nm thick GaAs spacer layer on either side, that is sandwiched between two 50 nm

thick Al_{0.25}Ga_{0.75}As barrier layers, all of which is grown on top of a 400 nm thick GaAs buffer on a n^+ -GaAs (100) substrate and capped by a 30 nm thick GaAs layer. The GaAs buffer and cap and AlGaAs barriers are grown at 590 °C and the substrate temperature is ramped down (up) without interruption during the growth of the first (second) 50 nm GaAs spacer to the much lower 490 °C growth temperature of the active region.

The V/III flux ratios ($F_{\text{As/Ga}}$ and $F_{\text{Sb/Ga}}$) used during the GaAsSb layer growth are $F_{\text{As/Ga}}=0.90$, with $F_{\text{Sb/Ga}}$ varying from 0.2 to 0.4 for the first set of PL samples, and $F_{\text{As/Ga}}=1.0$, with $F_{\text{Sb/Ga}}$ varying from 1.0 to 5.0 for the second set of PL samples. The flux ratio used here is the ratio of the group-V flux rate over the group-III flux rate where both are in units of atoms per unit area per unit time. The GaAs growth rate was 15 nm/min and the P flux ratio was fixed during the growth of the GaAsP layers in both sets of PL samples. The Sb mole fraction of the GaAsSb active region is determined from the PL peak position and is plotted as a function of $F_{\text{Sb/Ga}}$ and $F_{\text{As/Ga}}$ in Fig. 2(a). The power law equation,

$$x_{\text{Si}} = [a(F_{\text{As/Ga}})^b / (F_{\text{Sb/Ga}})^c + 1]^{-1}, \quad (2)$$

is fit to the data (see solid curves), where x_{Sb} is the Sb mole fraction of the GaAs_{1-x}Sb_x layer, $F_{\text{As/Ga}}$ and $F_{\text{Sb/Ga}}$ are the As/Ga and Sb/Ga flux ratios, and a , b , and c are fitting parameters whose values are listed in the inset of Fig. 2(a).

Similarly, three sets of GaAsP PL samples with a GaAsP QW sandwiched between two AlGaAs barriers were grown at various V/III ratios ($F_{\text{P/Ga}}$ and $F_{\text{As/Ga}}$) to calibrate the GaAsP composition; the P mole fraction as function of $F_{\text{P/Ga}}$ and $F_{\text{As/Ga}}$ is shown in Fig. 2(b). Equation (2) (with $F_{\text{Sb/Ga}}$ replaced by $F_{\text{P/Ga}}$) is fit to the data (see solid curves) and the fitting parameters are listed in the inset of Fig. 2(b). These parameters provide insight into the incorporation efficiency of the two group-V elements during the growth of mixed As-Sb and mixed As-P ternaries. Of the three fitting parameters in Eq. (2), a and c are similar and b is larger than c for both GaAsSb and GaAsP; this result indicates that As incorporates more efficiently than either P or Sb. Furthermore, the difference between b and c for GaAsSb is much greater than that for GaAsP, indicating that Sb does not compete nearly as efficiently with As as P does.

The growth temperature of the active region is further optimized by comparing the room temperature PL peak intensity, PL linewidth, and pulsed threshold current density of broad-area EELs with triple-QW active regions (without GaAsP strain compensation) that were grown at various substrate temperatures. A plot of the measurement results versus growth temperature is shown in Fig. 3. All three curves, PL peak intensity (upper plot), PL linewidth (middle plot), and threshold current density (lower plot), concur that the optimal growth temperature is ~ 500 °C. Similar growth studies indicate that the optimal growth temperature for the five-layer, strain compensated, GaAsP/GaAs/GaAsSb/GaAs/GaAsP QW system is ~ 490 °C. The introduction of GaAsP strain compensation layers to GaAsSb/GaAs QWs

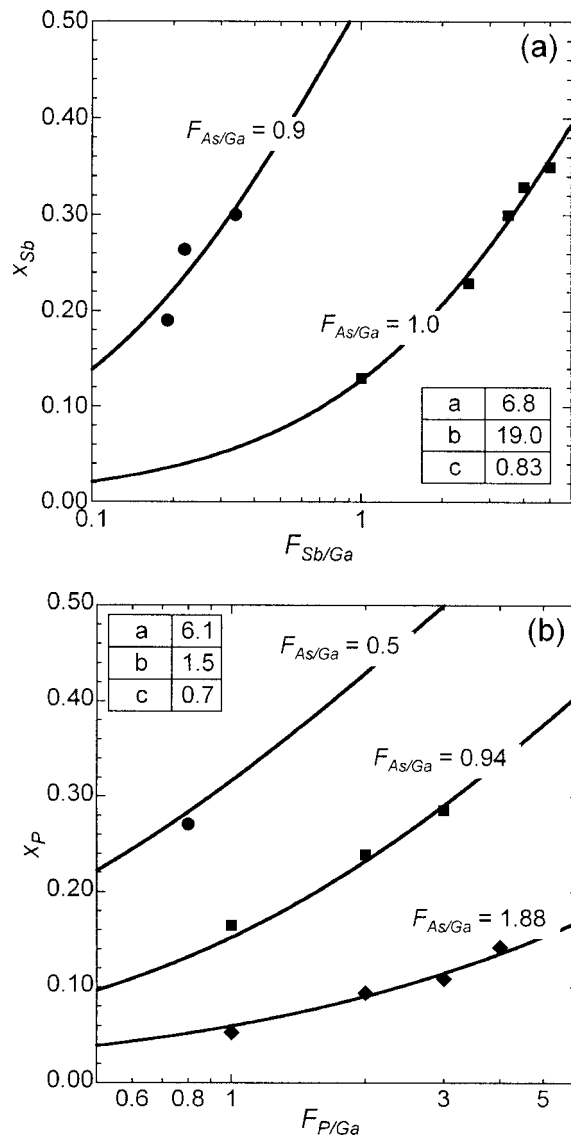


FIG. 2. (a) Sb mole fraction versus Sb/Ga and As/Ga flux ratios for MBE grown $\text{GaAs}_{1-x}\text{Sb}_x$ alloys. (b) P mole fraction versus P/Ga and As/Ga flux ratios for MBE grown $\text{GaAs}_{1-x}\text{P}_x$. The solid curves are fits of Eq. (2) to the data; the fitting parameters are listed in the table shown in each plot.

can reduce the PL linewidth by up to a factor of 2,¹⁴ indicating that the addition of strain compensation substantially reduces the strain-driven Sb segregation.

III. HIGH POWER, ROOM TEMPERATURE, CONTINUOUS-WAVE EDGE-EMITTING LASERS

Two high performance EEL devices, labeled A and B, are studied; these devices utilize strain compensated GaAsSb QWs grown under optimized growth conditions. The active region of device A (B) is a single (triple) $\text{GaAs}_{0.9}\text{P}_{0.1}/\text{GaAs}/\text{GaAs}_{0.7}\text{Sb}_{0.3}/\text{GaAs}/\text{GaAs}_{0.9}\text{P}_{0.1}$ QW with 8/3/7/3/8 nm (9/5/7/5/9 nm) thicknesses. The nominal Sb concentration is 30%, a value estimated from PL measurements and modeling. The active region in device A is sandwiched between two 78 nm thick $\text{Al}_{0.20}\text{Ga}_{0.75}\text{As}$ layers, followed by two 150 nm thick linearly graded AlGaAs lay-

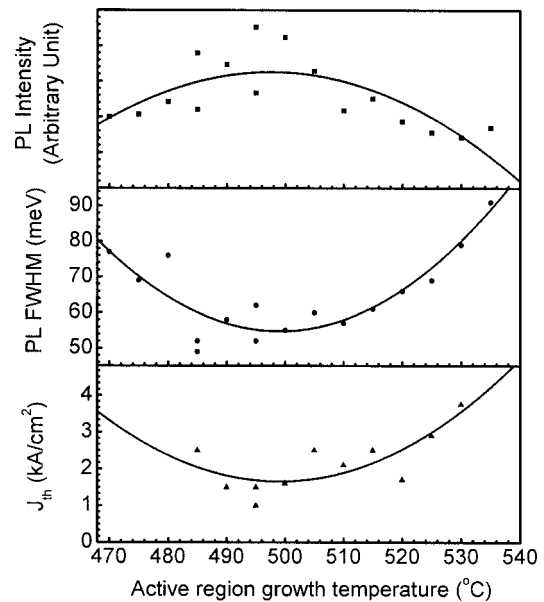


FIG. 3. EEL wafer PL intensity (upper plot), PL linewidth (middle plot), and threshold current density (lower plot) versus GaAsSb QW growth temperature.

ers, with Al mole fractions of 25%–65%, to form a graded-index (GRIN) waveguide, followed by a Si-doped ($2 \times 10^{18} \text{ cm}^{-3}$), 1.8 μm thick, *n*-type $\text{Al}_{0.65}\text{Ga}_{0.35}\text{As}$ cladding layer and a 500 nm thick GaAs buffer layer on the substrate side and a Be-doped ($2 \times 10^{18} \text{ cm}^{-3}$), 1.8 μm thick, *p*-type $\text{Al}_{0.65}\text{Ga}_{0.35}\text{As}$ cladding layer and a 100 nm thick GaAs contact layer on the surface side. The doping concentration is decreased from 2×10^{18} to $1 \times 10^{17} \text{ cm}^{-3}$ in both the *p* and *n* GRIN layers and is increased to $2 \times 10^{19} \text{ cm}^{-3}$ in the *p*-contact layer. Device B has a similar structure, except that the active region is sandwiched between two 20 nm $\text{Al}_{0.25}\text{Ga}_{0.75}\text{As}$ layers and both the *p*- and *n*-type $\text{Al}_{0.65}\text{Ga}_{0.35}\text{As}$ cladding layers are 2 μm thick.

The devices are fabricated using photolithography and inductively coupled plasma etching to define stripe ridges, ranging from 4 to 32 μm wide. By etching down to about 0.1 μm above the active region, these ridges provide current confinement as well as optical waveguiding. A photoresist mask is used to define the ridges, which also serves as a lift-off mask for the deposition of an Al_2O_3 isolation layer. This procedure ensures that a self-aligned contact window is exposed after lift-off. Wide Ti/Pt/Au *p*-contact stripes are deposited using a second mask, after which the wafers are lapped down to 100 μm thick and AuGe/Ni/Au *n*-metal contacts are deposited on the back side of the substrate; this is followed by rapid thermal annealing of both metal contacts. The wafers are cleaved to form EELs with various cavity lengths. The as-cleaved devices are mounted junction side up onto a temperature variable test stage. Room temperature pulsed measurements are performed using a 0.5 μs wide pulse and a 0.1% duty cycle. The power output is measured using a calibrated power meter equipped with an InGaAs detector and an integration sphere. Laser spectrum

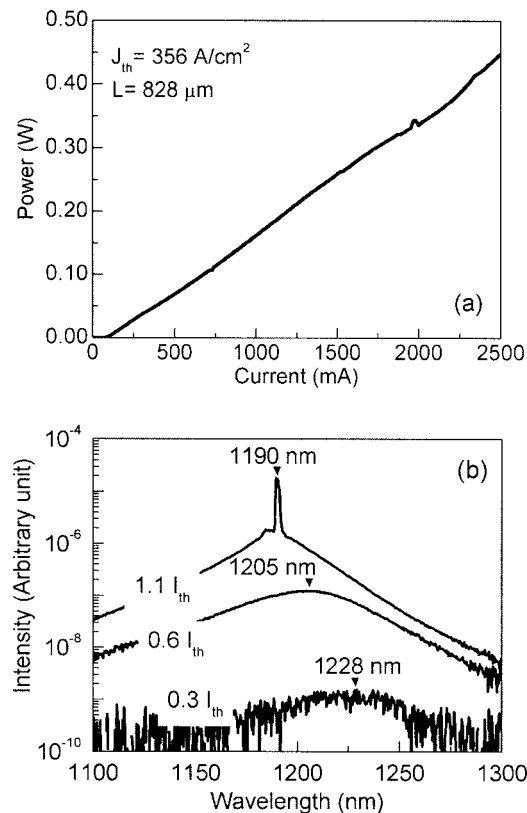


FIG. 4. Characterization results of a GaAsSb QW EEL with an 878 μm cavity length and a 32 μm ridge width. (a) Pulsed L - I curve (single facet). (b) Electroluminescence and lasing spectra.

measurements are performed using a 200 μm core diameter multimode fiber to couple the light into an ANDO 6315A optical spectrum analyzer.

A typical power-current (L - I) curve for device A (single QW) with an 878 μm cavity length and a 32 μm stripe width is given in Fig. 4(a). The device is driven by currents up to 2500 mA. The maximum output power is 0.45 W/facet, for a total 0.9 W output. The device has a threshold current (I_{th}) of 100 mA, which corresponds to a low threshold current density (J_{th}) of 356 A/cm². The small kink in the curve near 2000 mA is attributed to a detector measurement artifact due to a slow switching response during autoscaling. The emission spectra below threshold at 0.3 I_{th} and 0.6 I_{th} and just above threshold at 1.1 I_{th} are given in Fig. 4(b); the luminescence peak blueshifts from 1228 nm at 0.3 I_{th} to 1205 nm at 0.6 I_{th} and to 1190 nm at 1.1 I_{th} . Temperature dependent threshold current measurements between 0 and 85 $^{\circ}\text{C}$ exhibit a characteristic temperature of 60 K, which is close to previous reported results for this material system.^{5-7,10,12,16} Further temperature dependent device characterization work for this material system is reported in Ref. 16.

A typical cw L - I curve at 20 $^{\circ}\text{C}$ for device B (triple QWs) with a 935 μm cavity length and a 16 μm stripe width is given in Fig. 5; the power output measurements were limited by the detector to a maximum of 2 mW. The lasing threshold current density was 1.27 kA/cm². The 25 $^{\circ}\text{C}$ lasing spec-

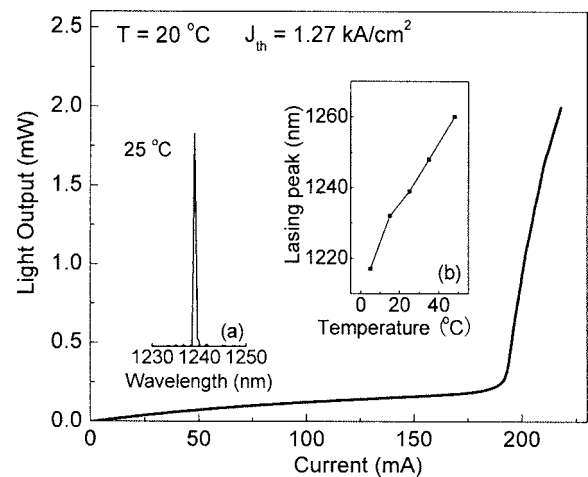


FIG. 5. L - I curve of a GaAsSb/GaAs QW EEL cw operating at 20 $^{\circ}\text{C}$ with a 935 μm cavity length and a 16 μm ridge width. Inset (a): threshold lasing spectrum at 25 $^{\circ}\text{C}$. Inset (b): threshold lasing wavelength as a function of temperature.

trum slightly above threshold is shown in Fig. 5, inset (a). This device exhibited a cw laser output up to 48 $^{\circ}\text{C}$ with wavelengths as long as 1260 nm. The threshold lasing wavelength increases from 1217 nm at 5 $^{\circ}\text{C}$ to 1260 nm at 48 $^{\circ}\text{C}$ [see Fig. 5, inset (b)]. This device also exhibits a significant blueshift under lasing operation; the room temperature PL peak wavelength is 1291 nm. This is the first reported GaAsSb/GaAs QW EEL with room temperature cw operation in the vicinity of 1.3 μm .

IV. ROOM TEMPERATURE CONTINUOUS-WAVE VCSELS

Top-emitting VCSELS utilizing the triple five-layer strain compensated GaAsSb/GaAs/GaAsP QWs were also studied. In these devices, the active region is placed at the center of a one λ cavity that is between the upper DBR of 23 pair Be-doped p -type Al_{0.9}Ga_{0.1}As/GaAs layers and the bottom DBR of 30.5 pair Si-doped n -type Al_{0.9}Ga_{0.1}As/GaAs layers. A 50 nm thick p -type AlAs oxidation layer is placed $3\lambda/4$ away from the cavity center in the p -DBR. Reflectance measurements were used to characterize the cavity mode of the as-grown wafer. PL measurements were performed by first etching away the top DBR so that the 514 nm Ar⁺ laser can directly pump the active region. The VCSELS were fabricated using standard photolithography and wet etching to define square (120 \times 120 μm^2) mesas. The mesa etch went down through the p -DBR layer and was stopped 0.1 μm above the active region to expose the oxidation layer. Selective wet oxidation of the AlAs layer was performed in a steam environment to form an $\sim 5 \times 7 \mu\text{m}^2$ current confinement aperture. A Ti/Au p contact was deposited on top of the mesa and a AuGe/Ni/Au n contact was deposited on the back side of the substrate. Finally, the devices were annealed at 400 $^{\circ}\text{C}$ for 30 s to form Ohmic contacts.

The devices were tested under cw operation at room temperature and exhibited peak powers ranging from 0.03 to 0.2 mW at wavelengths ranging from 1290 to

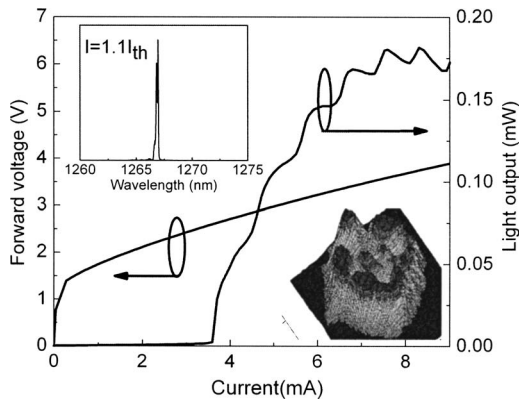


FIG. 6. GaAsSb VCSEL L - I - V curve; the lasing spectrum at 1.1 times threshold is shown in the upper-left inset; the near field lasing profile is shown in the lower-right inset.

1240 nm, respectively, depending on where the device was located on the wafer. Figure 6 shows the light-current-voltage (L - I - V) characteristics and lasing spectrum (upper-left inset) at 1.1 times threshold. The threshold current, turn-on voltage, and peak power are 3.7 mA, 1.5 V, and 0.18 mW, respectively. The ripples in the L - I curve are due to the optical feedback from the polished back side of the substrate. A three-dimensional near field image is shown in the lower-right inset of Fig. 6 and indicates that this VCSEL operates in a high order mode.

Three VCSELs labeled C, D, and E were studied with respective PL peak and lasing cavity-mode wavelengths of 1278 and 1260 nm (18 nm PL redshift), 1266 and 1285 nm (19 nm PL blueshift), and 1291 and 1260 nm (31 nm PL redshift) (see Table I). The lasing cavity-mode wavelengths are estimated from the cw lasing wavelengths. The device characteristics were determined using temperature dependent pulsed L - I measurements over a 0–90 °C range. The lasing threshold current versus temperature exhibits very different tuning characteristics for these three VCSELs; the results are given in Fig. 7 for device C (upper plot), device D (middle plot), and device E (lower plot). For device C, the threshold current increases slightly as the temperature increases from 0 to 60 °C and the threshold increases steeply from 60 to 80 °C. For device D, the threshold current decreases from 0 to 80 °C. For device E, the threshold decreases from 0 to 10 °C, is constant from 10 to 60 °C, and increases from 60 to 90 °C.

TABLE I. Summary of device PL peak, cavity mode, and PL peak redshift to cavity mode for devices C, D, and E.

VCSEL	PL peak (nm)	Cavity mode (nm)	PL peak redshift to cavity mode (nm)
C	1278	1260	18
D	1266	1285	-19
E	1291	1260	31

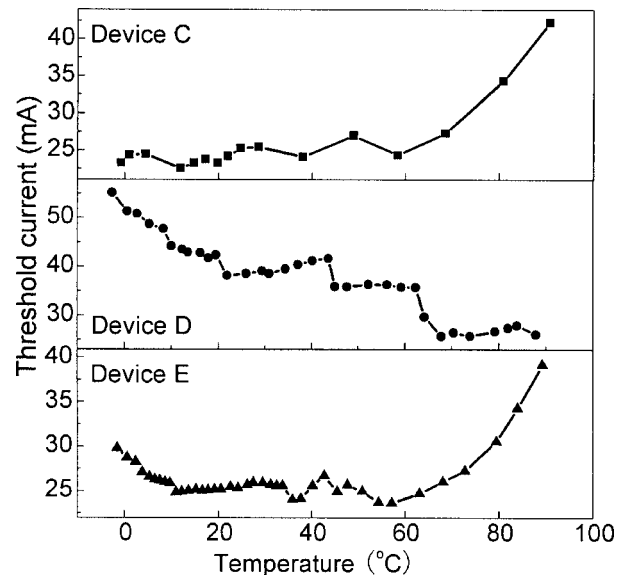


FIG. 7. Pulsed threshold current versus heat-sink temperature for three different GaAsSb QW VCSELs.

V. DISCUSSION

For the GaAsSb/GaAs material system, the gain peak is substantially blueshifted relative to the PL peak under injection due to strong band filling and inhomogeneous Sb composition,¹⁶ which is confirmed by the EEL results reported above. The different VCSEL threshold temperature characteristics shown in Fig. 7 are attributed to a combination of this blueshift and different initial gain-peak cavity-mode alignments; all devices tested were grown using the same recipe and processed back to back, and therefore similar electrical characteristics are expected. The room temperature PL peak relative to the cavity mode for devices C and E is redshifted by 18 and 31 nm, respectively. Consequently, the blueshift during lasing moves the gain peak toward the cavity mode, resulting in a low, temperature insensitive, threshold region from 10 to 60 °C where the gain peak and the cavity mode are nearly aligned. Conversely, the room temperature PL peak relative to the cavity mode for device D is blueshifted by 19 nm. Consequently, the blueshift during lasing moves the gain peak even further away from the cavity mode, resulting in a high, temperature sensitive, threshold that continually improves from 0 to 90 °C as the thermal redshift continually moves the gain peak toward the cavity mode. These results indicate that the room temperature PL peak should be redshifted by 20–30 nm relative to the cavity mode for optimal pulsed performance. However, under cw operation, it is estimated that the active region temperature is ~40 °C higher than the heat-sink temperature, causing a redshift of ~15 nm and a correspondingly reduced PL peak redshift for best room temperature cw performance.

The gain-peak blueshift also contributes to the high order transverse mode operation shown in the lower-right inset of Fig. 6. For oxide confined VCSELs, there are two distinct cavity modes: one at the longer wavelengths specified by the as-grown cavity length that lies within the oxide aperture and

one at the shorter wavelengths specified by the shorter cavity length in the region outside the oxide aperture, where the high refractive index AlAs layer has been converted to a low refractive index (optically thinner) Al₂O₃ layer. The spatial distribution of the modal gain at longer wavelengths conforms to the oxide aperture profile, which tends to support the single fundamental mode, provided that the aperture size is small (typically $10 \times 10 \mu\text{m}^2$ for GaAs or InGaAs based VCSELs), while at shorter wavelengths the profile is ring-like, which tends to support high order transverse modes. Therefore, when the peak modal gain at shorter wavelengths is larger (due to the above mentioned blueshift), the high order transverse mode will prevail (assuming the same optical losses for both modes). For the VCSEL shown in Fig. 6, the room temperature PL peak was close to the cavity mode, resulting in a blueshifted misalignment of the gain peak and cavity mode during lasing operation; this is expected to be the reason why this device exhibits a high order transverse modal behavior even though the oxide aperture is small.

These distinctive gain properties of the GaAsSb material system require a different design rule for VCSELs. In order to have good gain-peak cavity-mode alignment during room temperature lasing, it is essential that the room temperature PL peak be at substantially longer wavelengths than the cavity mode.

VI. CONCLUSIONS

The MBE growth of GaAsSb containing active regions is optimized by performing temperature dependent photoluminescence intensity, linewidth, and threshold current density measurements on edge-emitting lasers. The optimal growth temperatures are found to be 490 °C for strain compensated GaAsSb/GaAs/GaAsP active regions and 500 °C for GaAsSb/GaAs active regions. High performance edge-emitting lasers and vertical-cavity surface-emitting lasers are demonstrated using the strain compensated active region. The edge emitters demonstrated power outputs up to 0.9 W and threshold current densities as low as 356 A/cm² under pulsed operation and wavelengths as long as 1260 nm at temperatures up to 48 °C under cw operation. All edge-

emitting lasers displayed a strong gain-peak blueshift under high injection. The oxide confined VCSELs demonstrated room temperature cw operation with power outputs from 0.03 to 0.2 mW and lasing wavelengths from 1240 to 1290 nm. A room temperature PL peak redshift of 20–30 nm relative to the cavity mode provides the best pulsed operation performance for GaAsSb VCSELs.

ACKNOWLEDGMENT

This work is partially supported by the National Science Foundation under Grant No. 0070125.

- ¹T. Anan, K. Nishi, S. Sugou, M. Yamada, K. Tokutome, and A. Gomyo, *Electron. Lett.* **34**, 2127 (1998).
- ²T. Anan, M. Yamada, K. Tokutome, S. Sugou, K. Nishi, and A. Kamei, *Electron. Lett.* **35**, 903 (1999).
- ³P. Dowd *et al.*, *Appl. Phys. Lett.* **75**, 1267 (1999).
- ⁴W. Braun *et al.*, *J. Appl. Phys.* **88**, 3004 (2000).
- ⁵O. Blum and J. F. Klem, *IEEE Photonics Technol. Lett.* **12**, 771 (2000).
- ⁶M. Yamada, T. Anan, K. Tokutome, A. Kamei, K. Nishi, and S. Sugou, *IEEE Photonics Technol. Lett.* **12**, 774 (2000).
- ⁷S. Ryu and P. D. Dapkus, *Electron. Lett.* **36**, 1387 (2000).
- ⁸T. Anan, M. Yamada, K. Nishi, K. Kurihara, K. Tokutome, A. Kamei, and S. Sugou, *Electron. Lett.* **37**, 566 (2001).
- ⁹F. Quochi, D. C. Kilper, J. E. Cunningham, M. Dinu, and J. Shah, *IEEE Photonics Technol. Lett.* **13**, 921 (2001).
- ¹⁰P.-W. Liu, M.-H. Lee, H.-H. Lin, and J.-R. Chen, *Electron. Lett.* **38**, 1354 (2002).
- ¹¹P. Dowd, S. R. Johnson, S. A. Feld, M. Adamczyk, S. A. Chaparro, J. Joseph, K. Hilgers, M. P. Horning, K. Shiralagi, and Y.-H. Zhang, *Electron. Lett.* **39**, 987 (2003).
- ¹²M. S. Noh, R. D. Dupuis, D. P. Bour, G. Walter, and N. Holonyak, *Appl. Phys. Lett.* **83**, 2530 (2003).
- ¹³J. F. Klem, O. Blum, S. R. Kurtz, I. J. Fritz, and K. D. Choquette, *J. Vac. Sci. Technol. B* **18**, 1605 (2000).
- ¹⁴S. R. Johnson *et al.*, *J. Vac. Sci. Technol. B* **19**, 1501 (2001).
- ¹⁵S. R. Johnson *et al.*, *J. Cryst. Growth* **251**, 521 (2003).
- ¹⁶S.-Q. Yu, X. Jin, S. R. Johnson, and Y.-H. Zhang, *J. Vac. Sci. Technol. B* **24**, 1617 (2006).
- ¹⁷J.-B. Wang *et al.*, *Phys. Rev. B* **70**, 195339 (2004).
- ¹⁸B. Tell, K. F. Brown-Goebeler, R. E. Leibenguth, F. M. Baez, and Y. H. Lee, *Appl. Phys. Lett.* **60**, 683 (1992).
- ¹⁹D. B. Young, J. W. Scott, F. H. Peters, M. G. Peters, M. L. Majewski, B. J. Thibeault, S. W. Corzine, and L. A. Coldren, *IEEE J. Quantum Electron.* **29**, 2013 (1993).
- ²⁰B. Lu, P. Zhou, J. Cheng, K. J. Malloy, and J. C. Zolper, *Appl. Phys. Lett.* **65**, 1337 (1994).
- ²¹J. W. Matthews and A. E. Blakeslee, *J. Cryst. Growth* **27**, 118 (1974).